

SCIENTIFIC PAPERS
OF THE UNIVERSITY OF PARDUBICE
Series A
Faculty of Chemical Technology
20 (2014)

**FORMATION AND PROPERTIES
OF STRONTIUM ZINC PYROPHOSPHATE**

Nataliia GORODYLOVA, Žaneta DOHNALOVÁ and Petra ŠULCOVÁ¹
Department of Inorganic Technology,
The University of Pardubice, CZ–532 10 Pardubice

Received November 26, 2013

In present research we focused on the synthesis and investigation of properties of double strontium(II) zinc(II) phosphate — $SrZnP_2O_7$. Different synthesis approaches, including solid state reaction and coprecipitation, as well as different experimental conditions (initial reagents and homogenisation route) were used for the preparation of $SrZnP_2O_7$. The reaction route between the initial reagents was followed using DTA/TG and XRD methods. The obtained powders were characterised by IR spectroscopy and their thermal stability was followed by heating microscopy. Focusing on pigmentary application, specific properties of the samples were evaluated such as particle size distribution, colour parameters, and also preliminary anticorrosion tests were performed.

¹ To whom correspondence should be addressed.

Introduction

One of the important objects of investigation in modern material science is complex oxide compounds, where various functional materials already were found and adapted for actual technical needs as lasers, optical and magnetic materials, superconductors, ion conductors, semiconductors, sorbents, dielectrics, catalysts, pigments, etc. Among their variability, complex phosphates have an important role. The area of their application constantly increases due to the characteristic unique spectra of valuable chemical and physical properties, which depend on their composition and crystal structure [1-7].

Attention of our research group is focused on synthesis, characterization and pigmentary application of mixed phosphates [4,8] and, in particular, in the present work, the formation and properties of SrZnP_2O_7 are described. Previously, this composition was investigated as low temperature co-fired dielectric ceramics, and it was shown to be promising for application in mobile communication technology [9,10]. Such characteristics, as high quality factor value ($Q \times f$), low dielectric permittivity and low sintering temperature make SrZnP_2O_7 a suitable candidate for application as electrically tunable dielectric composite material in tunable microwave devices [11]. Effective absorption in the UV spectral region, high quantum efficiency and excellent chemical stability make phosphates suitable material for development of LED phosphors. In particular, SrZnP_2O_7 doped by $\text{Mn}^{2+}/\text{Eu}^{2+}$ or Eu^{2+} is considered as a potential excellent blue-red or violet-blue emitting phosphor for UV-LEDs and lamps for photo-therapy [6,7,12]. Moreover, it is well known, that phosphate compounds have a great role in the development of environmentally friendly inorganic pigments with anticorrosion properties [13-17]. The topic has been of high interest since the last few decades due to high toxicity of commonly used lead and chromate compounds [13,18-21]. Few generations of phosphate based anticorrosion pigments were developed [13,22-29], but there are only scarce examples of the investigation of pyrophosphate compounds as corrosion inhibitors [26,28]. In particular, our previous research reveals great potential of the related compound (SrMgP_2O_7) for application in anticorrosion paints [8], thus, expanded research in this area is required. Considering important role of Zn in corrosion inhibition and commercial application of zinc phosphates in pigmentary field, in the present work we focus on strontium zinc pyrophosphate. SrZnP_2O_7 samples obtained by different synthesis approaches in the combination with different experimental conditions, and their properties were characterised focusing on the potential application of this composition as corrosion inhibitor.

Experimental

Samples of mixed zinc strontium pyrophosphate were obtained using several synthesis approaches and different combinations of initial reagents. The solid state reaction upgraded by wet ball-milling in acetone was performed with the following starting compounds: $(\text{ZnCO}_3)_2 \cdot (\text{Zn}(\text{OH})_2)_3$ (P., Lachema, CZ), SrCO_3 (P., Lachema, CZ) and $(\text{NH}_4)_2\text{HPO}_4$ (P.A., Lachema, CZ). The homogenization procedure was performed in an agate form with agate balls placed in a planetary mill (Pulverisette 5, Fritsch, Germany). An appropriate amount of acetone was added in order to obtain a thick suspension. Rotation speed of 200 rpm was employed and the homogenization time was 1 h. After the homogenization procedure, the obtained suspension was completely dried in open air. The following calcination schedule was chosen for thermal processing of the samples: continuous heating ($5\text{ }^\circ\text{C min}^{-1}$) to $200\text{ }^\circ\text{C}$ maintained for 1 h, to $500\text{ }^\circ\text{C}$ maintained for 1 h, to $750\text{ }^\circ\text{C}$ maintained for 8 h; regrinding and final heating ($10\text{ }^\circ\text{C min}^{-1}$) to $900\text{ }^\circ\text{C}$ maintained for 8 h (sample I, Table I). After the calcination, the samples were thoroughly ground in an agate mortar with a pestle.

Table I Sample marking, initial reagents and synthesis conditions

Sample	Initial reagents	Homogenisation route	Thermal treatment schedule
I	$(\text{ZnCO}_3)_2 \cdot (\text{Zn}(\text{OH})_2)_3(\text{s})$ $\text{SrCO}_3(\text{s})$ $(\text{NH}_4)_2\text{HPO}_4(\text{s})$	Ball-milling in acetone	Drying $25\text{ }^\circ\text{C}/60\text{ h}$; calcination $200\text{ }^\circ\text{C}/1\text{ h}$; $500\text{ }^\circ\text{C}/1\text{ h}$; $750\text{ }^\circ\text{C}/8\text{ h}$; regrinding; calcination $900\text{ }^\circ\text{C}/8\text{ h}$.
II	$(\text{ZnCO}_3)_2 \cdot (\text{Zn}(\text{OH})_2)_3(\text{s})$ $\text{SrCO}_3(\text{s})$ $\text{H}_3\text{PO}_4(\text{aq})$	Hand-milling	Drying $70\text{ }^\circ\text{C}/6\text{ h}$; calcination $200\text{ }^\circ\text{C}/1\text{ h}$; $500\text{ }^\circ\text{C}/1\text{ h}$; $750\text{ }^\circ\text{C}/8\text{ h}$; regrinding; calcination $900\text{ }^\circ\text{C}/8\text{ h}$.
III	$\text{Zn}(\text{NO}_3)_2(\text{aq})$, $\text{Sr}(\text{NO}_3)_2(\text{aq})$, $\text{H}_3\text{PO}_4(\text{aq})$, $\text{NH}_4\text{OH}(\text{aq})$	Coprecipitation	Drying $80\text{ }^\circ\text{C}/6\text{ h}$; calcination $200\text{ }^\circ\text{C}/1\text{ h}$; $500\text{ }^\circ\text{C}/1\text{ h}$; $750\text{ }^\circ\text{C}/8\text{ h}$; regrinding; calcination $900\text{ }^\circ\text{C}/8\text{ h}$.

Another reaction was performed using a different phosphate source, namely H_3PO_4 (P.A., Lachema, CZ) (sample II, Table I). The acid was added dropwise to a thoroughly homogenised mixture of $(\text{ZnCO}_3)_2 \cdot (\text{Zn}(\text{OH})_2)_3$ and SrCO_3 in an agate mortar. A white thick suspension formed after mixing of the initial reagents was dried at $70\text{ }^\circ\text{C}$ during 6 h and then ground. The resultant powder was calcinated

under the same conditions as in the previous case.

The next employed synthesis route was co-precipitation from aqueous solutions (sample III, Table I). In this case, firstly 1M solutions of $\text{Zn}(\text{NO}_3)_2$ (P.A., Lachema, CZ) and $\text{Sr}(\text{NO}_3)_2$ (P., MLchemica, CZ) and H_3PO_4 (P.A., Lachema, CZ) were prepared. Phosphoric acid was added dropwise to the mixture of Zn- and Sr-solutions with continuous stirring at the room temperature. Aqueous ammonia (P.A., Penta, CZ) was used to adjust pH value in the range of 7.5-8.5. The obtained coprecipitate was left to age for 1 day, then filtered, washed and dried at 80 °C for 6 h and calcinated. The calcination temperature schedule was similar to that of the previous samples.

Thermal behaviour of the reaction mixtures or dried coprecipitate was investigated using simultaneous differential thermal and thermo-gravimetric analysis (DTA/TG, Jupiter STA 449/C/6/F, Netzsch, Germany) in a temperature interval of 20-1000 °C, a heating rate of 10 °C min⁻¹, and $\alpha\text{-Al}_2\text{O}_3$ as reference material. The weight of samples was ~150 mg. X-Ray diffraction patterns were obtained using monochromatic CuK_α radiation and a scintillation detector (a diffractometer D8 Advance, Bruker, GB). Thermal stability was tested using a heating microscope with automatic image analysis in a temperature interval of 20-1000 °C and a heating rate of 10 °C min⁻¹ (EM201-12, Hesse Instruments, Germany; standard measurement uncertainty, typically ≤ 5 °C; calibrated using Sn, In, Al and Zn). For the measurement, samples were prepared as pellets of a cylindrical form with a diameter of 3mm, a height of 3mm and a mass of ~50-70 mg. The particle size distribution of the samples was measured using a laser scattering system and calculated based on Fraunhofer bending (Mastersizer 2000/MU, Malvern Instruments, UK). IR spectra of powders were recorded in the wave number range of 300-2000 cm⁻¹ (a spectrometer Specord M80, Carl Zeiss, Jena, Germany). The colour of the samples was evaluated by measurement of spectral reflectance in the visible region of light (400-700nm) using a ColorQuest XE (HunterLab, USA). The colour was measured for hand ground samples pressed into a cuvette. The measurement conditions for colour appearance were following: an illuminant D65, 10° complementary observer and measuring geometry d/8°. The colour properties are described in terms of CIE $L^*a^*b^*$ system (1976), where the values a^* (the axis red-green) and b^* (the axis yellow-blue) indicate the colour hue, the value L^* represents the lightness or darkness of the colour in relation to a neutral grey scale (it is described by numbers from zero (black) to hundred (white)). The parameter C^* (chroma) represents saturation of the colour $(a^{*2} + b^{*2})^{0.5}$ and h° represents the hue angle (arctangent $(b^*/a^* \times 360^\circ / (2 \times 3.14))$). For each colorimetric parameter of a sample, measurements were performed in triplicate, and an average value was chosen as its result. Generally, for a given sample, the standard deviation of the measured colorimetric parameters was < 0.10 and the relative standard deviation was ≤ 1 %, indicating that the measurement error can be ignored. With the aim to evaluate the performance of SrZnP_2O_7 as a

corrosion inhibition pigment, pH and the resistivity (ρ) of 10 % sample aqueous extracts were measured during 28 days. The specific conductivity (σ) was determined using a conductometer and pH — using a glass electrode (InoLab, WTW, Germany). The resistivity was calculated according to the relation $\rho = 1/\sigma$.

Results and Discussion

The phase composition of the synthesized powders was studied using X-Ray diffraction analysis. According to the obtained results, single phase of SrZnP_2O_7 was obtained in all the cases after the final calcination stage at 900 °C. Focusing on the phase composition, the influence of the synthesis conditions is nominal and each mentioned method allows obtaining of single phase powders. Moreover, at the middle stage after the calcination at 750 °C, the same intermediate products with a minor difference in peak intensities were detected — $\text{SrZn}_2(\text{PO}_4)_2$ and $\text{Sr}_2\text{P}_2\text{O}_7$. Thus, the reactivity followed the same path in all synthesis approaches, and the formation of SrZnP_2O_7 is accompanied by the same intermediate phases. In Fig. 1, as examples, XRD-patterns of sample I, which was calcinated at 750 and 900 °C, are presented. Better resolution of the diffraction lines of the sample, calcinated at 900 °C also indicates a better crystallinity of the final product [30].

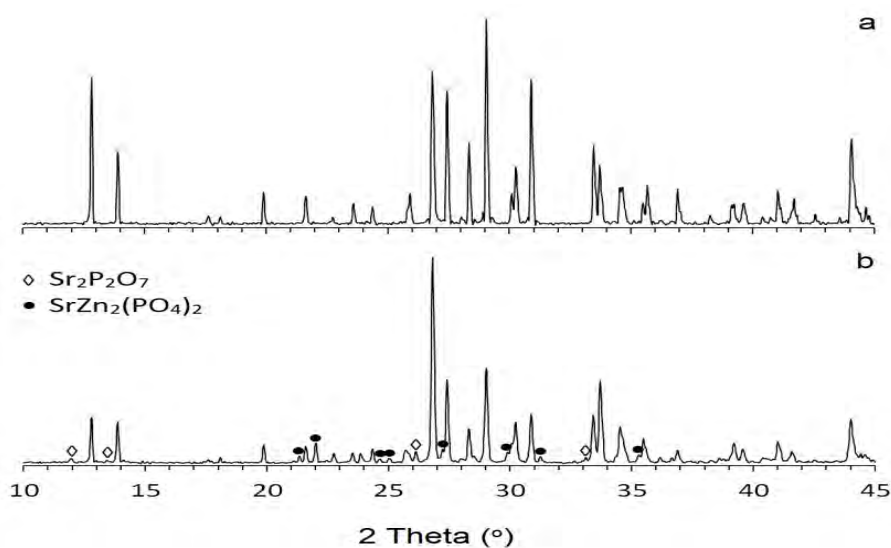
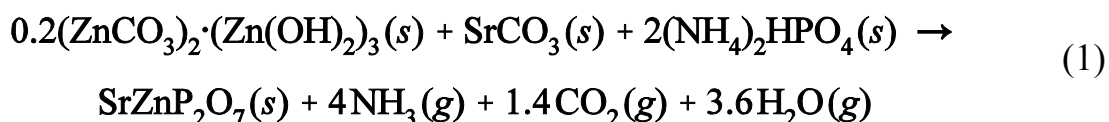


Fig. 1 XRD patterns of samples: a – sample I (900 °C); b – sample I (750 °C)

SrZnP_2O_7 was obtained previously by solid state reaction between SrCO_3 , ZnO and $(\text{NH}_4)_2\text{HPO}_4$ [10]. Ball milling in acetone was performed by the authors as a homogenisation procedure. In that case, the formation of SrZnP_2O_7 goes *via* different intermediate products than it is observed in our experiment. In particular, a mixture of pyrophosphates $\text{Sr}_2\text{P}_2\text{O}_7$, $\text{Zn}_2\text{P}_2\text{O}_7$ and SrZnP_2O_7 was observed by the authors at 850 °C which transforms in pure phase of SrZnP_2O_7 at 880 °C.

The structure of SrZnP₂O₇ belongs to the monoclinic syngony (P2₁/n space group) and the unit cell parameters are: $a = 5.3143(2) \text{ \AA}$, $b = 8.2080(3) \text{ \AA}$, $c = 12.7250(6) \text{ \AA}$, $\beta = 90.192(4)^\circ$, $V = 555.1(1) \text{ \AA}^3$, $Z = 4$. The single crystal structure of the pyrophosphate SrZnP₂O₇ was reported in 2007 by Höpfe *et al.* [12] and the Rietveld refinement by Yuan *et al.* [6]. In the structure, [ZnO₅] pyramids and [P₂O₇] groups connect with each other to form 3D-network by sharing the oxygen at the vertex of the polyhedral, and Sr²⁺ ions locate at the dodecahedra formed in the Zn-P-O network. P₂O₇-groups in this structure are characterized by staggered conformation, and cations are attributed to two crystallographically different positions depending on their size. SrZnP₂O₇ structure is highly related to α -CaP₂O₇ structure type. The family of isotypical pyrophosphates of general formula M^{II}SrP₂O₇, where M^{II} = Mg, Cr, Mn, Fe, Co, Ni, Cu and Zn, also adopts α -CaP₂O₇ structure type [31-36]. In general case, pyrophosphates with divalent ions can be divided into two main structure types: dichromate and thortveitite type, which are characterized, respectively, by eclipsed or staggered P₂O₇ conformation. Pyrophosphates with large cations (Ca, Sr, Ba, Pb, Cd) belong to the first group, and the second family includes related little cation pyrophosphates (Mg, Mn, Fe, Co, Ni, Cu, Zn) [31]. On its turn, the crystal structure of mixed pyrophosphates (dichromate or thortveitite type) is determined by a larger cation; nevertheless, some of them, in particular with Cu, adopt the thortveitite type, despite the expectation that a larger ion should dominate the selection of the dichromate structure. In the case of SrZnP₂O₇, this pyrophosphate is composed of two different-size cations, and its structure is determined by the larger one, Sr, and belongs to the dichromate family; however, the conformation of P₂O₇ anions is determined as staggered (antiperiplanar arrangement of the terminal PO₃ groups) [6,12].

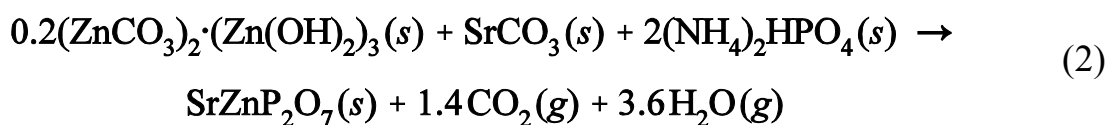
The differential thermal (DTA) and thermogravimetric (TG) analyses of the reaction mixtures and dried coprecipitate indicate exo- and endothermic effects with corresponding weight losses, accompanying the formation of SrZnP₂O₇. With regard to samples I, the TG curve detected a continuous weight loss up to 790 °C, while the DTA curve showed several endothermic effects (Fig. 1a). The formation of SrZnP₂O₇ in this case can be described by Eq. (1)



The endothermic effect started at ~90 °C and centred at ~200 °C corresponds to dehydration, deamination, dimerization and melting of (NH₄)₂HPO₄ and dehydration of (ZnCO₃)₂·(Zn(OH)₂)₃. The effect was accompanied by a weight loss of ~23 %. The theoretical weight loss connected with full dehydration and deamination of the starting compounds is 25.4 %, which is a little higher than the

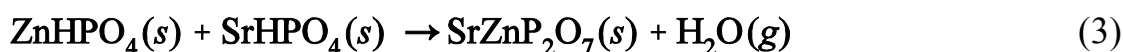
observed value. However, it is well known that in the discussed temperature range full dehydration of the phosphate component can not be achieved, thus the observed value of the weight loss is not in contradiction with the theoretical explanation. This endothermic process continuously passes into the next endothermic decarbonation of the initial carbonates accompanied by a weight loss of ~11 % in the temperature range of 230-340 °C. According to the theoretical calculations, the decarbonation of the initial carbonates must yield ~11.9 % (3.4 % of $(\text{ZnCO}_3)_2 \cdot (\text{Zn}(\text{OH})_2)_3$ and 8.5 % of SrCO_3). Taking into account a high temperature of the decomposition of SrCO_3 (above 1000 °C), it can be expected that at the temperature of 340 °C it is not complete and proceeds gradually until 790 °C. In addition, the gradual weight loss at higher temperatures (~3 % up to 790 °C) can be also explained by further dehydration of phosphate component. The general weight loss attained approximately 37.1 %, which precisely matches the value of 37.3 % calculated for this starting mixture. The endothermic decrease, which starts about 990 °C, corresponds to the melting of the sample.

A completely different behaviour was observed for the reaction mixture containing phosphoric acid after the drying stage. The general reaction of the formation of the double pyrophosphate starting from the employed reagents is presented in Eq. (2)



The initial weight loss (~ 6 %) accompanied by the endothermic effect with a minimum at 155 °C corresponds to dehydration and dimerization of orthophosphoric acid. The next step of the weight loss (~ 6 %) and the energy absorption (max. 263 °C) can be associated with reaction between carbonates and the phosphate accompanied by further dehydration and decarbonation processes, which stop only at ~ 835 °C. The general weight loss is about 15.4 %. Due to the drying stage of the initial suspension, the theoretical weight loss in this case is impossible to compare with the observed value. Similar to the previous case, an endothermic decrease, which starts about 930 °C, can be related to the melting of the sample.

In Fig. 1c, DTA-TG curves for sample III are presented. According to the literature data [37], in the case of precipitation using nitrates and orthophosphoric acid in this stoichiometry, a mixture of monohydrated ammonium metallophosphates ($\text{NH}_4\text{MPO}_4 \cdot \text{H}_2\text{O}$) is formed. In our case, interaction in the solution can be described by Eq. (3)



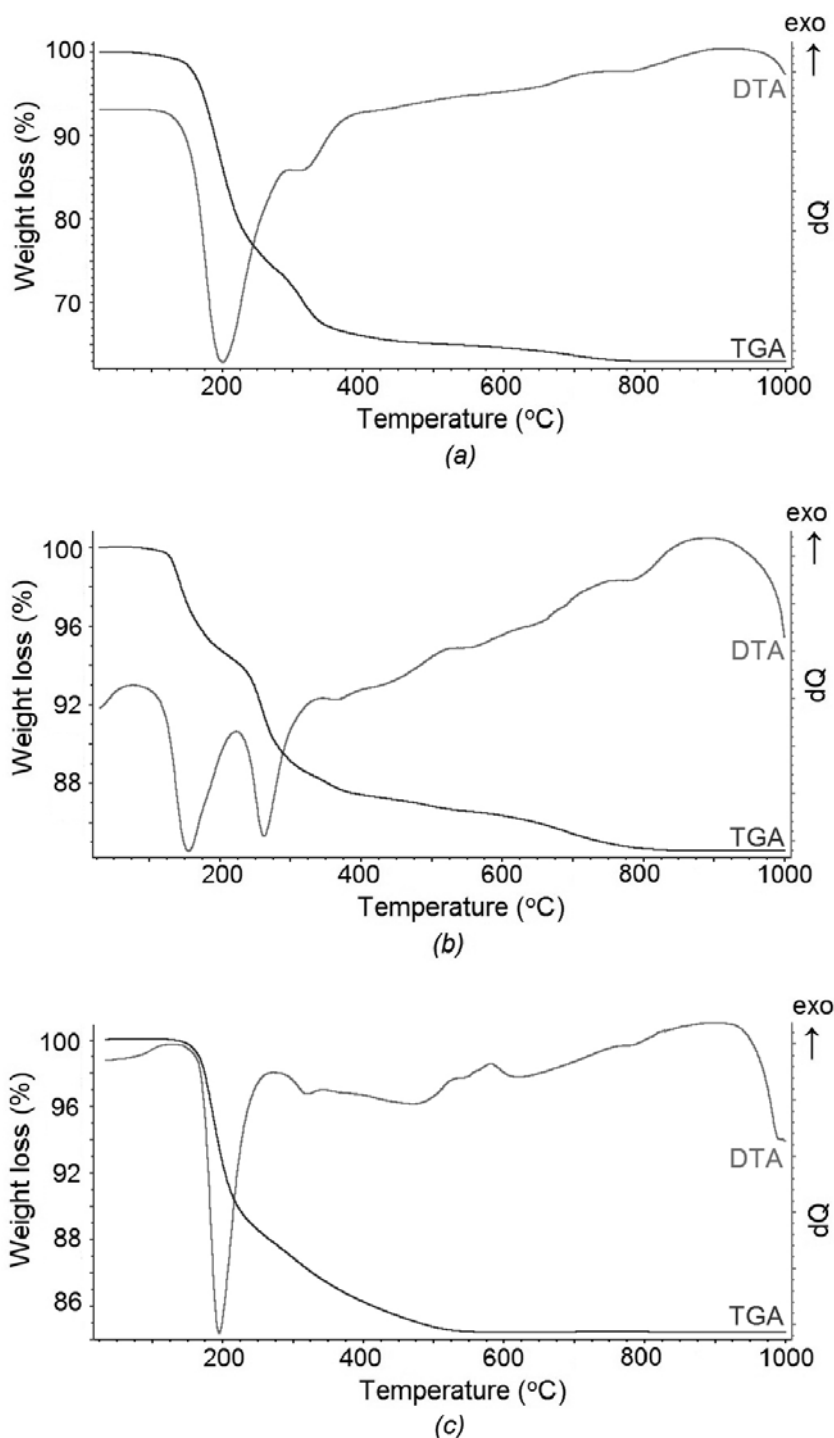
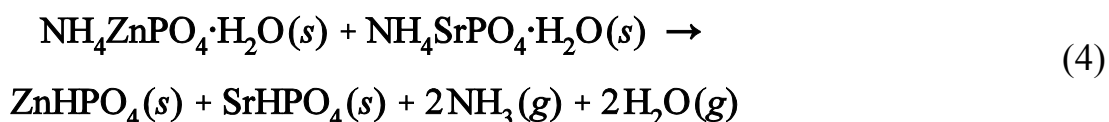


Fig. 2 DTA-TG investigation of initial mixtures: a – sample I; b – sample II (after drying stage); c – sample III (dried precipitate)

Accordingly, DTA/TG curves of raw powder present the decomposition processes of double ammonium phosphates. A strong endothermic effect between 150-250 °C with a minimum at ~195 °C corresponds to several overlapping steps, which are related to deamination and dehydration processes according to Eq. (4) with substantial associated weight loss of ~12 %.



The next gradual weight loss (up to 555 °C) corresponds to the further dimerization reaction with intermolecular dehydration leading to the formation of double pyrophosphate (Eq. (5)) and is accompanied by a gradual weight loss (~3.5 %). The calculated value for this process is 5.2 %, thus the difference can be explained by an incomplete deamination and dehydration in the previous stage. An endothermic decrease above 900 °C relates to the melting of the sample.



Calcinated powders were examined using a heating microscope on the subject of their thermal stability (Fig. 3). A significant value of sintering (down to 70 % of the area) was observed for all samples. This process started above 600 °C and finished with melting of the pellets. The melting point of SrZnP₂O₇ according to the thermal microscopy is about 1000 °C. The obtained value is in good agreement with DTA/TG analysis, where the endothermic effects were observed in this temperature area.

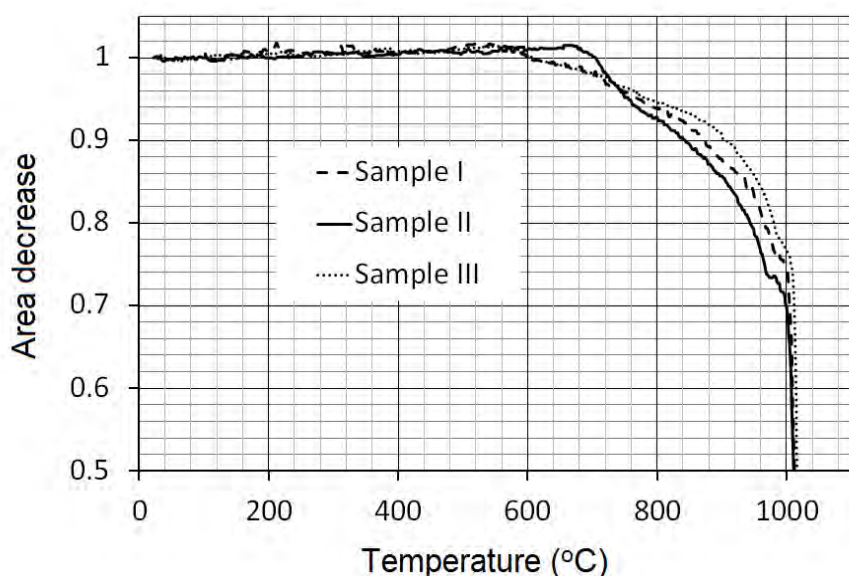


Fig. 3 Thermal behaviour of obtained samples

According to the measurement of the particle size distribution, the median size value ($d[50]$) for the powders, which were calcinated at 900 °C, highly depends on the synthesis conditions (Figs 4 and 5). The smallest particle size distribution was obtained for sample III of co-precipitated precursor ($d[50] = 19.76 \mu\text{m}$). Nevertheless, focusing on further anticorrosion application of the

samples, the obtained results are not satisfactory. Considering the requirements to anticorrosion pigment ($d[50] = 2-6 \mu\text{m}$), the obtained powders need additional milling. Milling was performed in agate milling forms in a laboratory planetary mill (200 rpm) during 20 min, and the determined particle size distribution for these samples matches the optimal range for their further application as pigments.

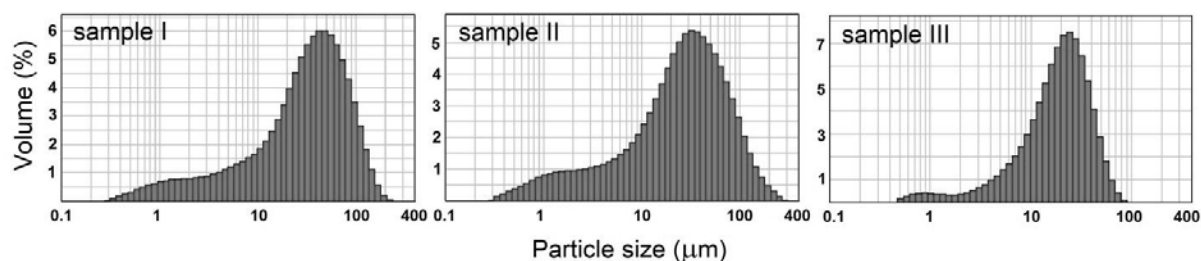


Fig. 4 Particle size distribution of obtained samples (I-III) in form of size bars on logarithmic scale

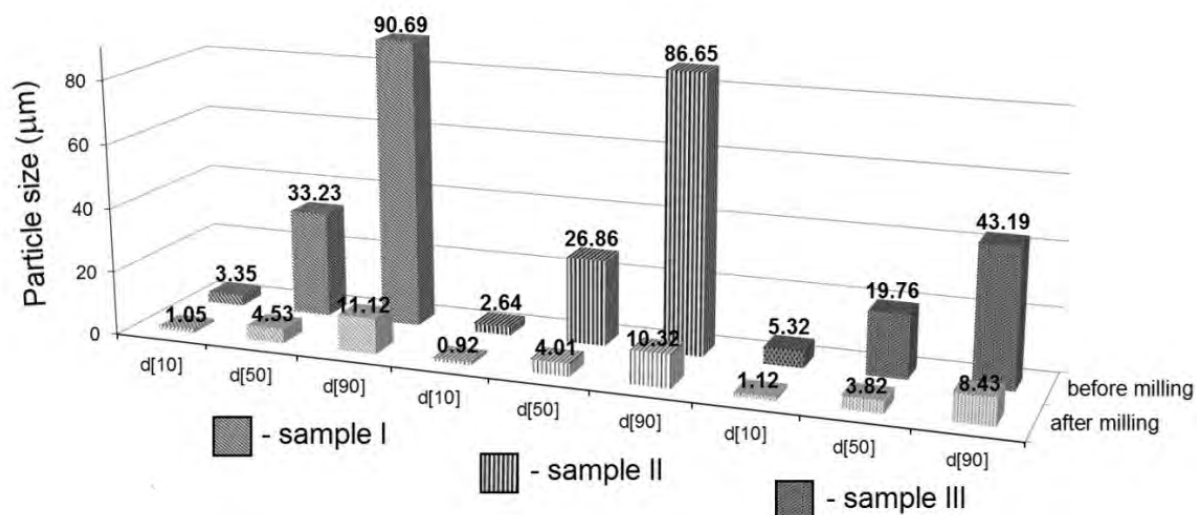


Fig. 5 Particle size diameters ($d[10]$, $d[50]$ and $d[90]$) of obtained samples (I-III) before and after the milling

In addition, infrared spectra of the obtained products were measured in order to confirm the phosphate functional group. As example, an IR spectrum of sample I (Fig. 6.) is presented in the finger-print region ($400-1500 \text{ cm}^{-1}$) of the absorption bands of the phosphate vibrations. The IR-spectrum absorption bands were attributed to P_2O_7 -group vibrations as follows: terminal stretching modes of the phosphate group appear in the range of $970-1180 \text{ cm}^{-1}$, and six deformation modes possibly coupled with some rocking modes of the phosphate group are not well resolved and are seen in the region of $500-640 \text{ cm}^{-1}$. Two absorption bands centred at 745 and 950 cm^{-1} correspond to the characteristic symmetric and antisymmetric bridge stretching modes, $\nu_s(\text{P-O-P})$ and $\nu_{as}(\text{P-O-P})$, respectively [38]. The width and the intensity of the antisymmetric mode can be explained by a large dipole

moment variation during the vibration. It can be related to the fact that the bridging oxygen is linked to one of the metal ions, which was previously observed for $M_2CdP_2O_7$ ($M = Li, Na, K, Rb, Cs$) [39]. The low-frequency band ($400\text{-}460\text{ cm}^{-1}$) observed in the spectrum can be controversially attributed to cationic motion or to deformation and rocking phosphate modes [38,39].

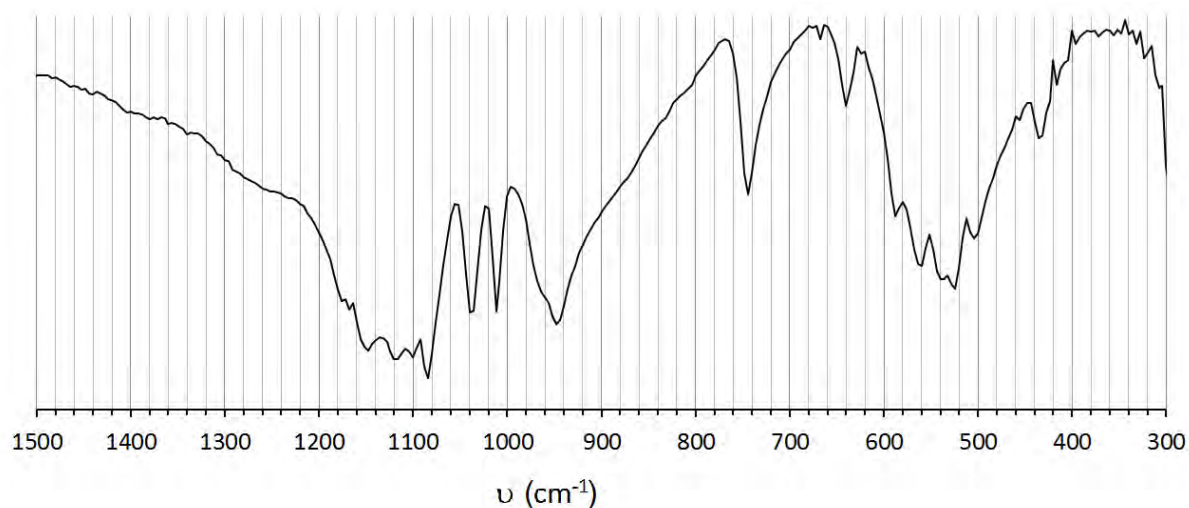


Fig. 6 IR-spectra of $SrMgP_2O_7$ (sample I, fired at $900\text{ }^\circ\text{C}$)

The colour parameters of the obtained samples were measured for hand-ground powders pressed manually into a quartz cuvette. The colour could be characterized as close to ideal white with high lightness ($L^* = 92.68\text{-}93.86$) and low values of the parameters a^* (-0.12 - -0.68) and b^* ($1.82\text{-}2.95$) (Table II). Low values of C^* indicate also very low saturation of the colour and hue angle — pale violet shade. Applied in an organic binder, these compounds form a semi-transparent cover, which can be explained by characteristic for phosphates low level of tinting strength and hiding power. With focus on the anticorrosion application, the colour of these samples is not a subject of main interest, because usually in anticorrosion paints additional colour pigments are used. However, these colour properties could be considered as an advantage, which allows to employ these compounds in the combination with any other colouring compositions in paints.

Table II Colour parameters of obtained samples

Sample	Colour parameters				
	L^*	a^*	b^*	C^*	h°
I	93.77	-0.12	2.03	2.03	273.35
II	93.86	-0.23	1.82	1.83	277.17
III	92.82	-0.31	1.91	1.93	279.18

Considering anticorrosion performance, anodic anticorrosion action of the phosphate pigments mainly consists in the formation of $\text{FePO}_4 \cdot 2\text{H}_2\text{O}$ insoluble film on the protected steel surface [13,15,18,42,43]. Thus, continuous solubility of SrZnP_2O_7 and, consequently, sufficient PO_4 -species concentration could provide high anticorrosion activity. On the other hand, the content of zinc and strontium and low solubility of the corresponding hydroxides of zinc and strontium could prevent cathodic disbondment and blistering of the protecting cover [18]. In current study, preliminary corrosion tests, including pH and the resistivity measurement of pigment aqueous extracts were performed. This procedure is intended to simulate the working conditions of the pigments and was employed only as a preliminary step [13,16,40-42]. The extracted solutions will be employed in future investigation to evaluate the corrosion rate of commercial carbon steel. pH and the resistivity (ρ) values of the 10% pigment suspensions are given in Table III.

Table III pH and the resistivity (ρ) measurement

Sample	1 day		28 days	
	pH	ρ , $\mu\Omega$ cm	pH	ρ , $\mu\Omega$ cm
I	6.58	0.0077	6.41	0.0046
II	6.73	0.0048	6.25	0.0031
III	6.72	0.0157	6.8	0.0085
water	5.78	1	-	-

During the aging process, a decrease in pH and the resistivity values was observed for almost all samples, with exception of sample III, where a slight increase in pH value from 6.72 to 6.8 was observed. It is worth to mention that pH value in the range of 7-9 is considered to be optimal for the best effectiveness of corrosion inhibitive pigments [18], but for the high anticorrosion efficiency of phosphates, according to literature data, the slightly acidic pH range is also suitable [13,42].

Concerning the resistivity of the obtained water extracts, these values are the criteria for evaluation of soluble species concentration, which is a very important parameter for characterization of phosphate corrosion inhibitors [15,42,43]. It is well known that their effectiveness is based on their partial solubility and on the formation of new compounds on the protecting cover. The synthesis method has a strong effect on the resistivity of the water extracts of the samples, and such different behaviour can be explained by different solubility of the samples. Thus, the presented data indicate that the preparation method has a significant influence on the solubility, which can seriously affect their inhibitor

activity. Probably it is connected with morphological characteristics, surface area, etc. which depend on the method of preparation. Taking into account the satisfactory pH and ρ values of the obtained samples, we can expect a high inhibitive efficiency, which will be verified in future anticorrosion tests with industrial steel plates and in paint application.

Conclusion

SrZnP_2O_7 was synthesized by different synthesis approaches and characterized using a set of techniques. The results of XRD analysis indicate that the different initial compounds and synthesis routes can be employed for synthesis of single-phase crystalline SrZnP_2O_7 . In general case, the formation of SrZnP_2O_7 followed the same path in all synthesis routes and is accompanied by the intermediate phases of $\text{SrZn}_2(\text{PO}_4)_2$ and $\text{Sr}_2\text{P}_2\text{O}_7$. The temperature of 900 °C is required to obtain the single-phase product. Thermal behaviour of the initial mixtures was followed by DTA/TG analysis. Observed endothermic effects and the weight loss are in agreement with the expected transformations in the mixtures during heating. The melting point of SrZnP_2O_7 according to the DTA/TG analysis and the thermal microscopy is about 1000 °C. A significant value of sintering (down to 70 % of the area) was observed for all samples above 600 °C. The particle size distribution of the powders highly depends on the synthesis conditions ($d[50] = 19.76\text{--}33.23$ μm) and 20 min of milling yield optimal value for their further application as anticorrosion pigments ($d[50] = 3.82\text{--}4.53$ μm). Observed bands in IR-spectra were attributed to stretching and deformation modes of the phosphate group, as well as to the characteristic symmetric and antisymmetric bridge stretching modes of pyrophosphate group. The colour of the obtained samples can be characterised as close to ideal white with high lightness and very low saturation. The data obtained for sample water extracts indicate that the preparation method has a significant influence on solubility of the powders, which can seriously affect their inhibitor activity. With respect to its application in the pigmentary field as an anticorrosion pigment, the obtained pH and in particular resistivity values indicate that SrZnP_2O_7 could be considered as a perspective corrosion-inhibitor.

Acknowledgement

The Ministry of Education, Youth and Sports of the Czech Republic, Project CZ.1.07/2.3.00/30.0021 “Enhancement of R&D Pools of Excellence at the University of Pardubice“, financially supported this work.

References

- [1] Bykov A.B., Chirkin A.P., Demyanets L.N., Doronin S.N., Genkina E.A., Ivanov A.K., Kondratyuk I.P., Maksimov B.A., Mel'nikov O.K., Muradyan L.N., Simonov V.I., Timofeeva V.A.: *Solid State Ion.* **38**, 31 (1990).
- [2] Scheetz B.E., Agrawal D.K., Breval E., Roy R.: *Waste Manage.* **14**, 489 (1994).
- [3] Roth M., Tseitlin M.: *J. Cryst. Growth* **312**, 1059 (2010).
- [4] Gorodylova N., Kosinová V., Dohnalová Ž., Bělina P., Šulcová P.: *Dyes Pigment.* **98**, 393 (2013).
- [5] Terebilenko K.V., Kirichok A.A., Baumer V.N., Sereduk M., Slobodyanik N.S., Gütlich P.: *J. Solid State Chem.* **183**, 1473 (2010).
- [6] Yuan J.L., Zeng X.Y., Zhao J.T., Zhang Zh.J., Chen H.H., Zhang G.B.: *J. Solid State Chem.* **180**, 3310 (2007).
- [7] Yang Zh.P., Yang G.W., Wang Sh.L., Tian J., Guo Q.L., Fu G.Sh.: *Chin. Phys. Lett.* **24**, 2094 (2007).
- [8] Gorodylova N., Dohnalová Ž., Šulcová P.: *J. Therm. Anal. Calorim.* **113**, 147 (2013).
- [9] Bian J.J., Kim D.W., Hong K.S.: *Mater. Res. Bull.* **40**, 2120 (2005).
- [10] Guo T., Wu W., Wang Y., Li Y.: *Ceram. Int.* **38S**, S187 (2012).
- [11] Jiang H., Zhai J., Yao X.: *J. Phys. D: Appl. Phys.* **42**, 225404 (2009).
- [12] Höpfe H.A., Daub M., Bröhmer M.C.: *Chem. Mater.* **19**, 6358 (2007).
- [13] Bethencourt M., Botana F.J., Marcos M., Osuna R.M., Sanchez-Amaya J.M.: *Prog. Org. Coat.* **46**, 280 (2003).
- [14] Masui T., Tategaki H., Furukawa S., Imanaka N.: *J. Ceram. Soc. Jpn.* **112**, 646 (2004).
- [15] Bělina P., Šulcová P., Trojan M., Mazurek P.: *Cent. Eur. J. Chem.* **5**, 706 (2007).
- [16] Bělina P., Myšková V., Šulcová P.: *J. Therm. Anal. Calorim.* **96**, 949 (2009).
- [17] Trojan M., Šulcová P., Mošner P.: *Dyes Pigment.* **44**, 161 (2000).
- [18] Sinko J.: *Prog. Org. Coat.* **42**, 267 (2001).
- [19] Martí M., Fabregat G., Azambuja D.S., Alemán C., Armelin E.: *Prog. Org. Coat.* **73**, 321 (2012).
- [20] Bethencourt M., Botana F.J., Calvino J.J., Marcos M., Rodríguez-Chacón M.A.: *Corrosion Sci.* **40**, 1803 (1998).
- [21] Yebra D.M., Kiil S., Dam-Johansen K.: *Prog. Org. Coat.* **50**, 75 (2004).
- [22] Naderi R., Attar M.M.: *Dyes Pigment.* **8**, 349 (2009).
- [23] Gerhard A., Bittner A.: *J. Coat. Technol.* **58**, 59 (1986).
- [24] Blustein G., Deyá M.C., Romagnoli R., del Amo B.: *Appl. Surf. Sci.* **252**, 1386 (2005).
- [25] Chromy L., Kaminska E.: *Prog. Org. Coat.* **18**, 319 (1990).

- [26] Deyá C., Blustein G., del Amo B., Romagnoli R.: *Prog. Org. Coat.* **69**, 1 (2010).
- [27] El-Hamid D., Blustein G., Deyá M., del Amo B., Romagnoli R.: *Mater. Chem. Phys.* **127**, 353 (2011).
- [28] Deyá M.C., Blustein G., Romagnoli R., del Amo B.: **150**, 133 (2002).
- [29] Veleva L., China J., del Amo B.: *Prog. Org. Coat.* **36**, 211 (1999).
- [30] Prevéy P.S.: *J. Therm. Spray Technol.* **9**, 369 (2000).
- [31] Boukhari A.: *J. Alloy Comp.* **188**, 14 (1992).
- [32] El-Bali B., Boukhari A., Aride J., Maass K., Wald D., Glaum R., Abraham F.: *Solid State Sci.* **3**, 669 (2001).
- [33] Maass K.: *New Studies about Quaternary Phosphates of Divalent 3d-Transition Metals*, Ph.D. thesis, Justus-Liebig University, Giessen, Germany, 2002.
- [34] Maass K., Glaum R., Gruehn R.: *Z. Anorg. Allg. Chem.* **627**, 2081 (2001).
- [35] Calvo C.: *Inorg. Chem.* **7**, 1345 (1968).
- [36] Tahiri A.A., El Bali B., Lachkar M., Ouarsal R., Zavalij P.Y.: *Acta Cryst.* **E58**, i9 (2002).
- [37] Llusar M., Garcia A., Gargori R., Galindo R., Badenes J.A., Monros G.: *J. Eur. Ceram. Soc.* **32**, 765 (2012).
- [38] Nakamoto K.: *Infrared and Raman Spectra of Inorganic and Coordination Compounds, Applications in Coordination, Organometallic, and Bioinorganic Chemistry, Part 2 of Infrared and Raman Spectra of Inorganic and Coordination Compounds*, John Wiley&Sons, New York, 2009.
- [39] Harcharra M., Ennaciri A., Rulmontb A., Gilbert B.: *Spectrochim. Acta A.* **53**, 345 (1997).
- [40] Trojan M.: *Dyes Pigment.* **13**, 1 (1990).
- [41] Czech technique norm, Corrosion of metals and alloys. Removal of corrosion products from specimens subjected to corrosion test, CSN ISO 8407 (038102), No17091, 1995.
- [42] Koopsmans A., Reijnders J.M.G.M.: *Proceedings of the 16th Fatipecc Congress.* **3**, 71 (1982).
- [43] Kalendová A.: *Anti-Corros. Method Mater.* **49**, 364 (2002).